ACS OMEGA

http://pubs.acs.org/journal/acsodf

Article

Cosolutes Modify Alkaline Phosphatase Catalysis through Osmotic Stress and Crowding Mechanisms

Oksana A. Yavorska, Lukas Syriste, Chantal M. du Plessis, Maryam Yaqoob, Kyle Loogman, Michael Cordara, and John K. Chik*

Cite This: *ACS Omega* 2021, 6, 26239−26250

Read Online

ACCESS | Metrics & More | Article Recommendations | Supporting Information

ABSTRACT: Examining the effects of different cosolutes on *in vitro* enzyme kinetics yielded glimpses into their potential behavior when functioning in their natural, complex, *in vivo* milieu. Viewing cosolute *in vitro* influences on a model enzyme, calf intestinal alkaline phosphatase, as a combination of competitive and uncompetitive behaviors provided quantitative insights into their effects on catalysis. Observed decreases in the apparent specificity constant, K_{asp}, caused by the presence of polyethylene glycols or betaine in the reaction solution, indicated interference with enzyme−substrate complex formation. This competitive inhibition appeared to be driven by osmotic stress. Dextran 6 K and sucrose strongly impeded the subsequent conversion of the bound substrate into a free product, which was marked by sharp reductions in V_{max}, uncompetitive inhibition. For the same step, smaller noncarbohydrate cosolutes, triethylene glycol, polyethylene glycol 400, and betaine, also behaved as uncompetitive inhibitors but to a lesser extent. However, polyethylene glycol 8000 and 20,000 were uncompetitive activators, increasing V_{max}. Polyethylene glycol of molecular weight 1000 displayed intermediate effects between these two groups of noncarbohydrate cosolutes. These results suggested that crowding has a strong influence on free product formation. The combination of competitive and uncompetitive effects and mixed behaviors, caused by the cosolutes on calf intestinal alkaline phosphatase kinetics, was consistent with the trends seen in similar enzyme−cosolute studies. It is proposed that the double-displacement mechanism of alkaline phosphatases, shared by many other enzymes, could be the root of this general observation.

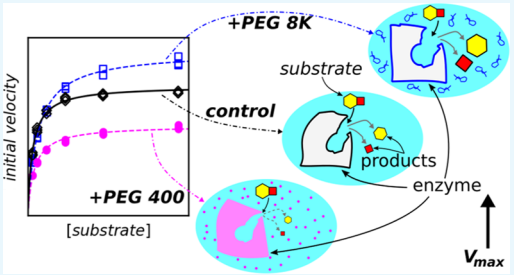

INTRODUCTION

In contrast to the highly dilute solutions traditionally used in *in vitro* studies, enzymes evolved to function within densely filled, *in vivo* environments.[1,2] Inside *Escherichia coli*, cosolutes, such as proteins and nucleic acids, constitute approximately 30−40% by weight of the intracellular milieu.[3] Additionally, small-molecule metabolites are estimated to be present at a total concentration of 0.3 M.[4] Far from being inert, the presence of these nonbinding cosolutes is felt in many biochemical processes including enzyme kinetics.[5−8] A better understanding of how these complex environments can modify enzyme activity will enable better prediction of actual *in vivo* behavior from *in vitro* data.

When treated as hard spheres or rectangular parallelepipeds in a continuum solvent, cosolutes modify enzyme activity through crowding and the reduction of volume available for proteins to function.[8,9] Crowding particularly affects steps involving significant volume changes through alterations in shape or assembly. For enzymes, this is especially the case when ligands are similarly sized, resulting in substantial volume or shape changes upon enzyme−substrate complex formation and product release. The binding of much smaller ligands is not expected to induce sufficient shape or volume change on the enzyme to be markedly affected by crowding.[9] Crowding is also predicted to be important when the enzyme exists as an equilibrium of different oligomeric states each with unique kinetic properties, as observed for glyceraldehyde-3-phosphate dehydrogenase (GAPDH), which exists in an equilibrium between tetrameric, dimeric, and monomeric forms.[10] Kinetic rate constants associated with transition state incurring significant shape or volume change should also be susceptible to crowding.[8,9] Crowding effects strongly depend on both the fraction of volume occupied by the cosolute/crowder and their relative shape and size. This property is valuable when trying to distinguish whether crowding is at work when using polymeric cosolutes.[5] While crowding drives systems to adopt more compact states, often with higher symmetries, in the related concept of confinement, systems favor conformations that better match the "architecture" of the crowded milieu. The complex environment results in systems taking on a smaller

Received: June 21, 2021
Accepted: September 16, 2021
Published: September 30, 2021

https://doi.org/10.1021/acsomega.1c03243
ACS Omega 2021, 6, 26239−26250

conformational subset than those in dilute solutions that may not be the most compact.[8,11]

Although hard-sphere modeling provided several important insights, it omits many chemical details of the cosolutes themselves. In osmotic stress[12] and preferential hydration,[13] the nonbinding chemical nature is expressed as the degree of cosolute exclusion from the immediate enzyme vicinity. This exclusion leads to enhanced or preferential hydration near their surfaces. Hard-sphere models also lead to preferential surface hydration through steric interference, leading to depletion forces.[14,15] The centrality of cosolute surface exclusion in these different mechanisms is a manifestation of the Gibbs−Duhem equation.[16] Solution osmotic pressure is the central parameter in osmotic stress measurements and replaces the volume occupied and relative cosolute size in hard-sphere models. The competition for water, as more osmotic pressure is applied, results in the system favoring the more dehydrated state. The osmotic stress approach has yielded insights across a diverse set of molecular biological systems such as channels,[17] protein-DNA interactions,[18] the allosteric transition of hemoglobin,[19] and hexokinase kinetics.[20,21]

Cosolute-induced enzyme conformation changes would be an obvious means for altering protein function. Crowding by Ficoll 70 resulted in structural changes, monitored by FRET, of fluorescently modified phosphoglycerate kinase connected with enhanced enzyme activity.[22] Molecular simulations associated these observations with the relative movement of the enzyme domains. In other studies, the presence of crowding agents decreased the distances between fluorescent donor proteins connected by a flexible linker to fluorescent acceptor proteins, as measured by FRET.[23,24] This was attributed to crowding instead of confinement since the overlap concentration of Ficoll-70 was cited to be > 500 g/L. For hemoglobin, the presence of cosolutes osmotically favors the transition from its fully oxygenated, relaxed *R*-state to its more dehydrated, fully deoxygenated, tense *T*-state.[19] This transition was accompanied by a loss of ∼60 water molecules. Assuming that the cosolutes did not significantly alter the three-dimensional structures of these states, the calculated reduction in the accessible surface area was approximately 700 Å^2. This was also accompanied by a decrease of the apparent specific volume of 0.002 cm^3/g, a slight change given that the volume of methemoglobin is taken to be 0.748 cm^3/g.[25] This last example highlights the difference between crowding and osmotic stress, which stems from how to attribute the cause of the observed effects. From the osmotic stress point of view, the cosolute competing for available water results in systems favoring states of greater dehydration, leading to reduced accessible surface area and therefore a smaller volume. From the crowding perspective, adopting a smaller volume naturally leads to decreased accessible surface area and thus dehydration. Although the cause may be different, both osmotic stress and crowding essentially lead to an equivalent end point.[16] This is not necessarily the case for confinement where the complex solution environment could favor conformations with larger surface areas. Viewing cosolute effects through these different lenses provides contrasting insights into the mechanism of their action.

Employing a form of the Michaelis−Menten equation that uses V_{max} and K_{asp}, the apparent specificity constant, rather than the conventional V_{max} and K_m, facilitated leveraging concepts borrowed from reversible, small-molecule competitive and noncompetitive inhibitors to systematically quantitate cosolute effects on enzyme kinetics.[26,27] Like most previous enzyme−cosolute studies, the Michaelis−Menten kinetic scheme, described in Figure 1, was used for modeling catalysis.

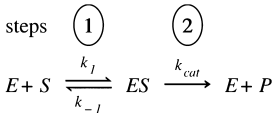

Figure 1. "Classic" first-order (or pseudo-first-order) Michaelis−Menten scheme. In step ①, the rate constants k_1 and k_{-1} represent the reversible binding and unbinding of the substrate, *S*, to the enzyme, *E*, forming the enzyme−substrate complex, ES. Step ② represents the conversion of the ES into free product, *P*, and the return of *E*. In the initial-rate assumption, where the product is absent, step ② is essentially "irreversible", and it is represented only by a forward rate constant, k_{cat}.

Combining the scheme in Figure 1 with the usual initial-rate and steady-state assumptions gives the familiar Michaelis−Menten equation in eq 1 describing the dependence of the initial velocity, v_0, on substrate concentration, [*S*].[26]

$$v_0([s]) = \frac{v_{max}[S]}{K_M + [S]} \tag{1}$$

K_M, the Michaelis constant, and V_{max} are given in eq 2.

$$K_M = \frac{k_{-1} + k_{cat}}{k_1} \qquad and\ V_{max} = E_T k_{cat} \tag{2}$$

E_T is the total concentration of the enzyme accounted for by the sum of [*E*] and [ES].

While V_{max} represents the asymptotic initial velocity at saturating substrate concentration, the change in v_0 at vanishingly small substrate concentration is given K_{asp}, defined in eq 1 (see Figure 1 from Johnson[27])

$$K_{asp} = \frac{V_{max}}{K_M} \tag{3}$$

Equation 1 can be easily transformed to use V_{max} and K_{asp}, as shown in eq 4.

$$v_0([S]) = \frac{K_{asp}[S]}{1 + (K_{asp}/V_{max})[S]} \tag{4}$$

However, unlike Johnson,[27] eq 4 retained V_{max} rather than normalizing it by E_t to give k_{cat} (eq 2) and converting K_{asp} into k_{cat}/K_M, the specificity constant.[26] Although the traditional Michaelis constant, K_M, is unambiguously the substrate concentration where $v_0 = V_{max}/2$, interpreting the significance behind changes in K_M is more complicated.[26] Furthermore, K_M is the least precise parameter compared with either V_{max} or K_{asp}.[26] Calculating the error in K_{asp} by propagating the standard deviation of V_{max} and K_M results in an exaggeration of the error versus fitting K_{asp} directly.[27]

An advantage of using eq 4 is that V_{max} and K_{asp} are ideally suited for interpreting cosolute effects as a mixture of competitive and uncompetitive behaviors. Pure competitive inhibitors exclusively interfere with step ① (Figure 1), preventing ES formation by competing with substrate binding. This lowers K_{asp} and leaves V_{max} unchanged since saturating the substrate will outcompete any finite amount of the inhibitor.[26] Pure uncompetitive inhibitors, on the other hand, bind specifically to already formed ES complexes, solely

https://doi.org/10.1021/acsomega.1c03243
ACS Omega 2021, 6, 26239−26250

preventing step ②, product formation, and release. This reduces V_{max}, while K_{asp} remains constant.[26] For mixed inhibitors, both V_{max} and K_{asp} decrease. In contrast, the effect of inhibitors on the V_{max} and K_M combinations of parameters is slightly more complex. Although for pure competitive inhibition, V_{max} remains constant and K_M increases, pure uncompetitive inhibition lowers both V_{max} and K_M proportionally.

Competitive, uncompetitive, and mixed behaviors are conveniently measured by calculating the ratio of K_{asp} and V_{max} in the absence and presence of inhibitors or cosolutes, α and α' respectively, as shown in eq 5.

$$\alpha = \frac{K_{asp}}{K^*_{asp}} = \frac{V_{max}/K_M}{V^*_{asp}/K^*_M} \qquad \text{and } \alpha = \frac{V_{asp}}{V^*_{asp}} \tag{5}$$

In eq 5, the asterisk (*) indicates the presence of inhibitors or cosolutes. For competitive inhibition, $\alpha > 1$ and $\alpha' = 1$, while for uncompetitive inhibition $\alpha = 1$ and $\alpha' > 1$. For mixed inhibitors, both α and α' would be greater than one.

The ratios, α, and α', also accommodate situations where cosolutes behave as activators,[26] increasing K_{asp}* or V_{asp}* relative to the dilute control. Activation results in α or α' being less than one. In this paper, competitive, uncompetitive, and mixed behavior refers to effects on steps ① or ②, independent of the form of their action, inhibition, or activation. In this regard, cosolute-induced mixed behaviors on enzyme kinetics could be divided into four subtypes depending on the α and α' ratios. These different subtypes are summarized in Table 1.

Table 1. Summary of the Different Cosolute-Induced Mixed Behaviors

behavior	subtypes	abbr.	α	α'
mixed	competitive inhibitor, uncompetitive inhibitor	CIUI	>1	>1
	competitive activator, uncompetitive inhibitor	CAUI	<1	>1
	competitive inhibitor, uncompetitive activator	CIUA	>1	<1
	competitive activator, uncompetitive activator	CAUA	<1	<1

Using α and α' enables examination of cosolute effects on the different steps in the Michaelis–Menten scheme (Figure 1). Finally, it is essential to emphasize that although the concepts from reversible inhibition are being used to quantitate cosolute effects, it is not implied nor required that the cosolutes directly bind to the enzyme or the enzyme–substrate complex.

Alkaline phosphatases (APs) are ubiquitous dimeric metallophosphomonoesterases that retain a high degree of sequence similarity despite their occurrence in diverse species from *E. coli* to humans.[28] One significant difference between the highly studied AP from *E. coli* versus mammalian AP is the latter's well-documented uncompetitive inhibition by amino acids such as L-leucine and L-phenylalanine, L-phe.[29] This property is attributed to an approximately 30-amino-acid insert which forms the "crown" domain observed in the mammalian AP structures.[30,31] Intestinal alkaline phosphatase (IAP) is one of four related, tissue-specific mammalian isozymes, with the others being placental, germline, and tissue-nonspecific.[32] The calf-intestinal form (CIAP), whose expression vanishes in mature animals,[33] is noted for its high activity.[28] Like most studies on AP, the assay reaction used was the hydrolysis of para-nitrophenyl phosphate, PNPP, into free phosphate, Pi, and para-nitrophenol, PNP, shown in Figure 2.

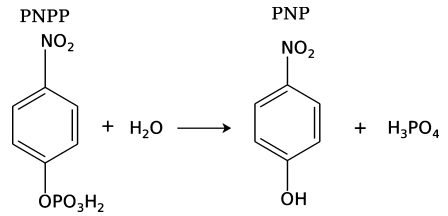

Figure 2. Hydrolysis of PNPP to PNP and free phosphate, Pi.

PNP absorbance around 400 nm was used to follow the reaction progress.

RESULTS

Effects of 30% PEG 400 Versus 30% PEG 8 K on CIAP Catalysis—A Specific Example. Figure 3 demonstrated the success of modeling the effects of 30% (w/w) polyethylene glycol, PEG, molecular weight 400, and PEG, molecular weight 8 K, on CIAP kinetics using eq 4. It justified leveraging the concepts of competitive and uncompetitive behaviors to quantitatively contrast the influences of these cosolutes.

Table 2 shows the V_{max}, K_{asp}, and K_m values derived from Figure 3 data and the consequent α and α' values. At 30% concentration, both PEG 8 K and PEG 400 were competitive inhibitors, interfering with step ① and hence ES formation. This was evidenced by their reduced K_{asp} relative to dilute control. This resulted in $\alpha > 1$, with values of 1.63 and 1.9 for PEG 8 K and PEG 400, respectively (Table 2). However, their effect on step ② was opposite with PEG 8 K acting as an uncompetitive activator, causing an increase in V_{max} and leading to $\alpha' = 0.79 < 1$. PEG 400; on the other hand, was an uncompetitive inhibitor, decreasing V_{max} and resulting in $\alpha' = 1.44 > 1$ (Table 2). The effects of 30% PEG 8 K and PEG 400 on CIAP kinetics are examples of CIUA and CIUI mixed behavior (Table 1). Although 30% PEG 8 K increased K_M to a greater extent than PEG 400, 0.59 mM versus 0.38 mM, respectively, when changes in V_{max} are accounted for, PEG 400 emerged as a more potent competitive inhibitor, as quantitated by α, 1.9 versus 1.63 (Table 2). This underlined the advantages of interpreting changes in K_{asp} versus K_M and the general importance of collecting complete kinetic data versus single-substrate concentration activity measurements.

Overview of α and α' of Different Cosolutes. Like the above specific case of PEG 400 and PEG 8 K (Figure 3), the effects of all examined cosolutes on CIAP kinetics were well modeled by eq 4, supporting the use of α and α' to quantitate their effects. Figure 4 summarizes the α and α' versus wt % for the examined cosolutes.

From Figure 4A, TEG and all the PEGs exerted similar competitive inhibitory effects, $\alpha > 1$, on CIAP kinetics, independent of the wide range of molecular weights used, from 150 Da for TEG to PEG 20 kDa. However, their uncompetitive behavior displayed a striking mass dependency (Figure 4C). Smaller PEGs, TEG, and PEG 400, behaved as uncompetitive inhibitors, reducing V_{max}, $\alpha' > 1$, with similar concentration dependence. In contrast, the larger PEGs, PEG 8 K and 20 K, increased V_{max}, $\alpha' < 1$, making them uncompetitive activators. From Table 1, the smaller PEGs exhibited CIUI mixed behavior, while larger PEGs were CIUA.

https://doi.org/10.1021/acsomega.1c03243
ACS Omega 2021, 6, 26239−26250

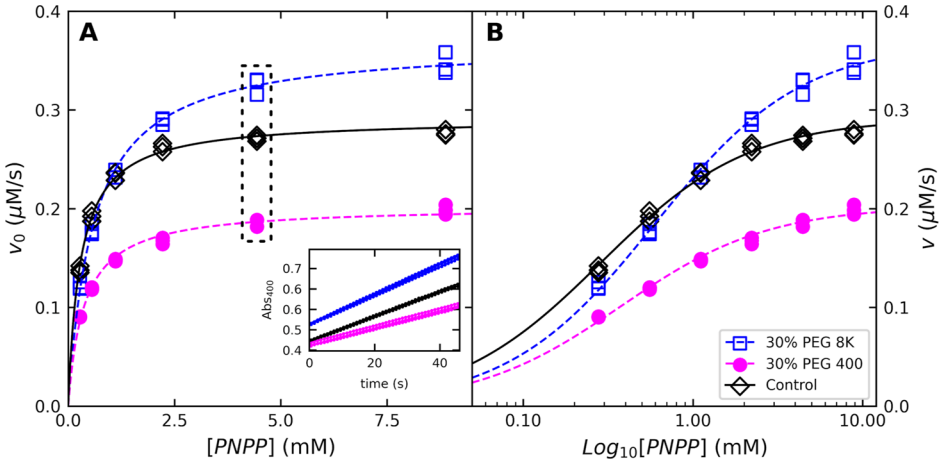

Figure 3. Effects of 30% PEG 8 K versus 30% PEG 400 on the initial velocity of PNPP hydrolysis catalyzed by CIAP. (A) Observed initial velocity of AP-catalyzed PNPP hydrolysis versus substrate concentration under dilute/control conditions in 30% PEG 8 K and in 30% PEG 400 fitted to the Michaelis−Menten eq 4. [Insert shows the absorbance at 400 nm, Abs_{400}, versus time data used to determine the initial velocity at [PNPP] = 4.4 mM, highlighted in the dashed box.]; (B) same data in the main figure of panel A shown using a log scale for [PNPP]. The PNPP concentration range was 0.06−8.9 mM.

Table 2. V_{max}, K_{asp}, K_M, α, and α' Derived from Figure 1 Data

solution (w/w)	V_{max} (μM/s)[a]	Kasp ($\times 10^{-3}$/s)[a]	K_M (mM)[b]	SSR[c]	α[d]	α'[d]
control	0.291 ± 0.002	1.01 ± 0.03	0.28 ± 0.01	0.00042		
30% PEG 8 K	0.367 ± 0.004	0.62 ± 0.02	0.59 ± 0.02	0.000069	1.63 ± 0.07	0.79 ± 0.01
30% PEG 400	0.202 ± 0.002	0.54 ± 0.02	0.38 ± 0.02	0.00036	1.9 ± 0.1	1.44 ± 0.02

[a]Values of parameters ±standard deviation fitting data to eq 4. [b]Value of K_m ± standard deviation fitted to eq 1. Fitting to either eq 1 or eq 4 did not significantly alter V_{max}. [c]Sum of squares residues of the fit to eq 4. Number of observations = 18 for each solution. [d]Values ± error estimate. Error calculated by propagating standard deviation of fitted K_{asp} and V_{max}, respectively.

PEG 1 K began to show uncompetitive inhibition ($\alpha' > 1$) at high concentration, CIUI. Otherwise, PEG 1 K appeared to act as a pure competitive inhibitor and served as a "boundary" separating uncompetitive behaviors of the small and large PEGs.

Compared to the PEGs, sucrose and dextran 6 K, carbohydrate-based cosolutes, showed greater uncompetitive inhibition ($\alpha' > 1$) at similar concentrations compared to the glycols (Figure 4C,D), with dextran 6 K displaying the strongest uncompetitive inhibition. These significant decreases in V_{max} made it more challenging to measure K_{asp} reliably, contributing to the scatter in α displayed in Figure 4B. Both sucrose and dextran 6 K appeared to show similar competitive behavior. Much of the α values tended to be scattered around one and perhaps trending toward being less than one, suggesting that sucrose and dextran 6 K could act as competitive inhibitors at low concentrations before becoming activators with increasing wt %. Overall, dextran 6 K and sucrose appear to behave largely as uncompetitive inhibitors. Lastly, betaine, a neutral zwitterion, acted as a CIUI mixed inhibitor with more significant competitive inhibition than the PEGs at similar concentrations and similar uncompetitive inhibition to the small PEGs (Figure 4B,D).

Figure 5 shows the same α and α' data in Figure 4 from the osmotic stress perspective. The similarity in the correlation between α and log(Π) of PEG 20 K and PEG 8 K is highlighted by the heavy dashed blue line in Figure 5A. PEG 1 K initially followed a similar trend with PEG 20 K and PEG 8 K for log(Π) between 6.0 and 6.8. Beyond this region, PEG 1 K and the other smaller, noncarbohydrate-based cosolutes required greater osmotic pressure to reach the same degree of competitive inhibition as PEG 8 K and 20 K, as highlighted by the black dashed box in Figure 5A. The data points for the smaller cosolutes such as TEG and betaine appear in the right-hand part of the box, and the larger cosolutes occupy the left region. As previously mentioned, the strong uncompetitive inhibition by dextran 6 K and sucrose led to inconclusive scattering around $\alpha = 1$ across the full range of log(Π) examined.

In contrast, Figure 5B, showing α' versus log(Π), highlighted the molecular mass-based segregation of noncarbohydrate cosolutes into uncompetitive activators and inhibitors, as well as the starkly stronger uncompetitive inhibition by carbohydrate cosolutes. PEG 20 K and PEG 8 K exhibited similar uncompetitive activator behavior across their combined osmotic pressure range. Increased V_{max} in the presence of larger PEGs (8 K and 20 K) was also observed by Sekiguchi et al.[34] for bovine intestinal AP. However, this was accompanied by increased specificity constant ($\alpha < 1$), competitive activation, which could be a result of the difference in solution pH (9.8 vs. 8.8 in this study).[34] Over a similar log(Π) range, the small PEG's and betaine acted as uncompetitive inhibitors. At log(Π) below 6.2, PEG 1 K initially appeared to behave as an uncompetitive activator, like PEG 20 K and PEG 8 K, before joining the other small noncarbohydrate cosolutes as an uncompetitive inhibitor. The larger dextran 6 K was a more potent uncompetitive inhibitor compared to sucrose. Although, it should be noted that the osmotic pressure data of dextran T10,[35] used in place of dextran 6 K, should be slightly lower than the actual osmotic pressure. A similar size-dependent effect of carbohydrate cosolutes has been previously reported by Homchaudhuri et al.[36] At concentrations between 0.25 and

https://doi.org/10.1021/acsomega.1c03243
ACS Omega 2021, 6, 26239−26250

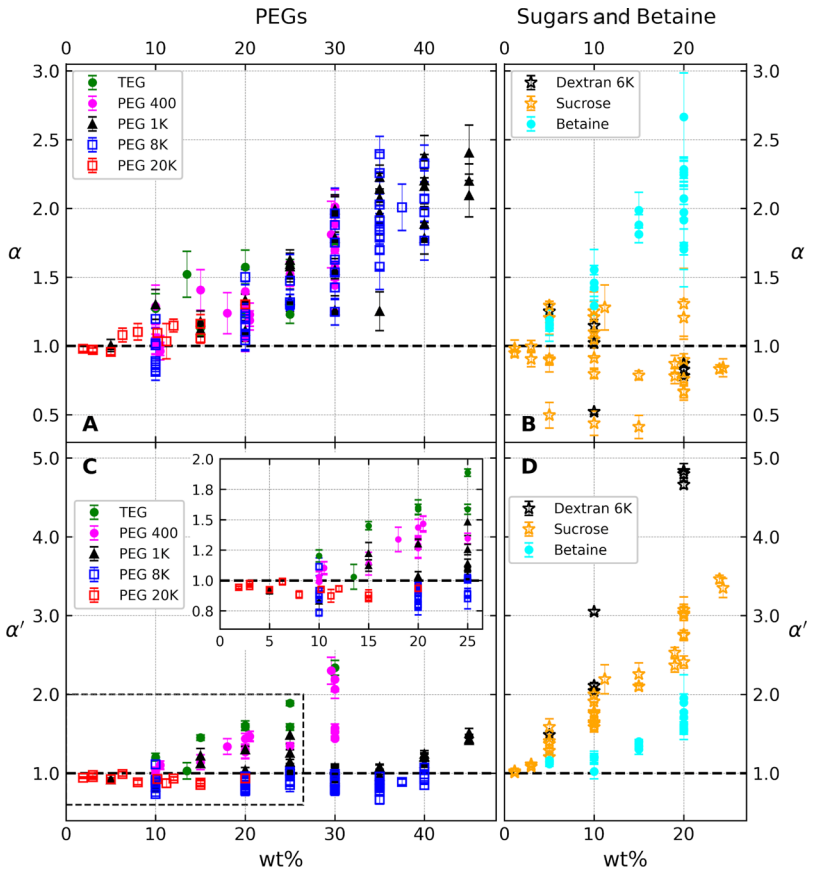

Figure 4. Effects of different concentrations of various cosolutes on CIAP kinetics, as quantitated by α and α'. The heavy, dashed, horizontal line in all panels represents α or α' equal to 1 (i.e., no change). Error bars represent the estimated error in α and α' calculated by propagating the standard deviations of V_{max} and K_{asp}. (A) α versus weight % (wt %) of triethylene glycol (TEG), PEG 400, 1, 8, and 20 K molecular weight. (B) α versus wt % of betaine, sucrose, and dextran 6 K molecular weight. (C) α' versus wt % of TEG, PEG 400, 1, 8, and 20 K molecular weight [insert: an enlargement of the dotted rectangle region in panel C. Axes are the same as in panel C]. (D) α' versus wt % of betaine, sucrose, and dextran 6 K molecular weight. Data files of the V_{max} and K_{asp} values determined by fitting data to eq 4, and V_{max} and K_M values by fitting to eq 1 are found in Supporting Information, All Data-Kasp-csv.txt and AllData-Km-csv.txt, respectively.

1 M, sucrose has also been reported to be a noncompetitive inhibitor on human placental alkaline phosphatase.[37] Noncompetitive inhibition is a particular case of CIUI, where $\alpha = \alpha' > 1$.

Overview of Kinetic Data Collected in the Absence of Cosolutes. Quantitating cosolute-induced changes in CIAP kinetics as the relative change in K_{asp}, α, and V_{max}, α', provided an insightful framework for interpreting these alterations. Equally important, it facilitated combining data from several researchers, six undergraduate students, and one faculty member, over a 6 year period. Figure 6 shows V_{max} versus K_{asp} and K_m from the 73 dilute control results by all contributors.

As seen in Figure 6, the spread in V_{max}, K_{asp}, and K_M stems largely from variation between individual authors rather than within a single contributor. The larger error bars for K_M compared to both V_{max} and K_{asp} in Figure 6B and C are consistent with K_M being the least well-defined parameter compared to K_{asp} and V_{max}.[26] This is further demonstrated in Supporting Information Figure S1 showing the histograms of the relative error of each of these variables.

DISCUSSION

Different Steps in the Michaelis–Menten Scheme Were Affected by Different Mechanisms. Viewing cosolute effects through the lens of crowding and osmotic stress provides contrasting perspectives on their mechanism. The qualitative similarity between α versus log(Π) of the noncarbohydrate cosolutes in Figure 5A combined with the largely molecular weight-independent relationship between α versus wt % of the same cosolutes (Figure 4A,B), and the inconclusive competitive inhibition from sucrose and dextran 6 K suggested that step ① (Figure 1) was primarily sensitive to osmotic stress from the noncarbohydrate cosolutes. The small volume change expected from PNPP (MW 217 Da) binding to the significantly larger CIAP dimer (MW 140 KDa) predicted that crowding should have little influence on this step. AP monomers also dimerize spontaneously with few free monomers remaining,[38] making crowding-induced changes in oligomerization, as observed for GAPDH,[10] an unlikely contributing factor. The molecular weight attenuation highlighted by the dashed box in Figure 5A could be attributed to the decreased exclusion of smaller cosolutes from the immediate enzyme environment compared to larger cosolutes. The greater inclusion of smaller cosolutes near the enzyme requires larger concentrations away from the enzyme to generate the same net difference in cosolute concentration.[16] This size-dependent exclusion has been observed in alamethicin ion channel conductance,[39] in glucose binding to hexokinase,[20,21] and in the radius of gyration and hydration of

https://doi.org/10.1021/acsomega.1c03243
ACS Omega 2021, 6, 26239−26250

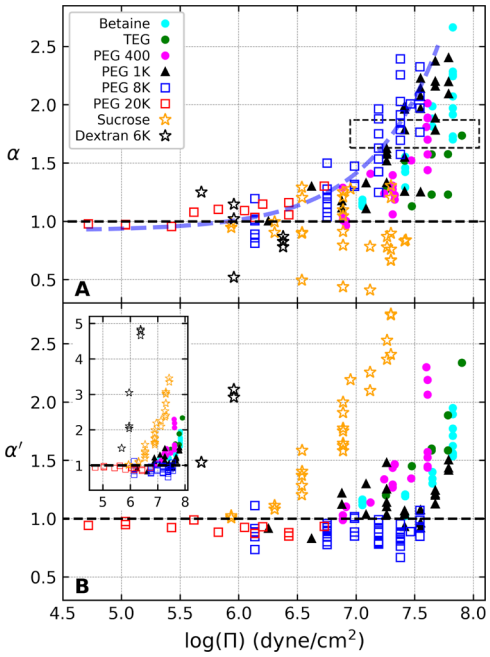

Figure 5. Data from Figure 4 replotted as a function of the logarithm of cosolute osmotic pressure (in dyne/cm^2), log(Π). For clarity, the error bars have been omitted. (A) α versus log(Π). The heavy blue dashed line is an exponential fit to PEG 20 K and PEG 8 K data and serves only as a visual guide (see text). The region around α = 1.75 is indicated by the box outlined with a black dashed line (see text). (B) α' versus log(Π). The insert shows the entire data set. The insert axes are the same as in the main panel figure.

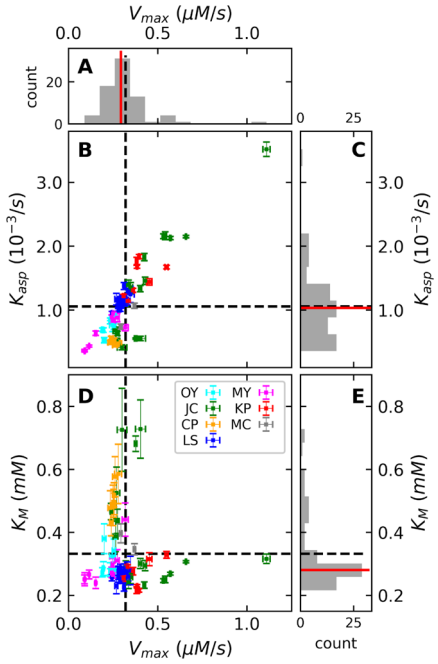

Figure 6. V_{max} versus K_{asp} and K_m for control data by the authors of this paper. The horizontal and vertical dashed black lines represent the mean of K_M and V_{max}, respectively, and the median of the histograms is shown by the solid red line. The error bars represent one standard deviation of the fitted parameters. (A) Histogram of V_{max} determined from fitting data to eq 4. Mean = 0.319 ± 0.138 μM/s. Median = 0.293 μM/s. (B) V_{max} versus K_{asp} based on fitting to eq 4. (C) Histogram of K_{asp} determined from fitting to eq 4. Mean = 1.06 ± 0.54 × 10^{-3}/s. Median = 1.04 × 10^{-3}/s. (D) V_{max} versus K_M determined from fitting data to eq 1. There was very little difference in V_{max} and its standard deviation using eq 1 versus eq 4 (E) Histogram of K_M determined from fitting to eq 1. Mean = 0.332 ± 0.119 mM. Median = 0.281 mM.

lysozyme and guanylate kinase.[40] Increasing osmotic stress favors the more dehydrated enzyme state resulting from the competition for water by cosolutes. The increase in competitive inhibition suggests that this drier state disfavors ES formation, which could result from closure or obstruction of the binding site, as proposed for hexokinase[20,21] and phosphoglycerate kinase.[22]

The effects of the examined cosolutes in step ②, uncompetitive behavior, presented a more complex situation where crowding was likely an important factor. Both dextran 6 K and sucrose exerted greater uncompetitive inhibition than the smaller PEGs and betaine when either as a function of wt % or log(Π) (Figures 4B,D and 5). Most strikingly, although PEG 400 and sucrose share very similar osmotic pressure versus wt % profiles (Figure S2 in Supporting Information), largely a result of their similar molecular weights, their effect on uncompetitive inhibition was very different in Figure 5B. This illustrates PEG's less-than-ideal crowding behavior compared to carbohydrates[8,41] due to its observed attractive and repulsive interactions beyond the basic hard-sphere potential.[42,43] The relatively weak competitive inhibition in the presence of sucrose and dextran 6 K compared to their uncompetitive behaviors further supports the idea that step ① was less affected by crowding (Figure 4). Also, the magnitude of these additional forces would scale with PEG size and possibly be the source behind their mass-dependent effects on competitive and uncompetitive behavior.[44,45] Figures 4D and 5B also highlight the enhanced uncompetitive inhibition by dextran 6 K. This could be due to confinement effects since Rong reported that the overlap concentration of dextran T10 was 22%,[46] which is in the range reported by Squire[47] and coincides with the highest dextran 6 K concentration examined, 20%, as seen in Figure 4D.

Although the strong uncompetitive inhibition by dextran 6 K and sucrose suggested that step ② was susceptible to crowding, the mechanism is unclear. Once bound, PNPP and the catalytic pocket should be shielded from the solvent and hence unaffected by cosolutes, as already noted for α-chymotrypsin.[48] Also, the catalytic step and release of small products should be accompanied by little notable volume change. These two issues make it difficult to attribute changes in k_{cat} to crowding. An alternative explanation would be to instead consider cosolute effects on E_t, the total enzyme concentration (eq 2). It has been suggested that the excluded volume by the cosolute would effectively increase the enzyme concentration, E_t.[6] Although this would account for increases in CIAP V_{max} from the larger PEGs, it alone does not completely explain the reduction in V_{max} from the smaller PEGs over the same wt % range nor the absence of progressive increases in V_{max} with greater wt % of large PEGs seen in Figure 4C,D. This "plateauing" of V_{max} with increased Ficoll concentration was also observed in EcoRV.[49] Pastor et al.[50] reported monotonic and dextran weight-independent decreases in V_{max} as a function of increased concentration for horseradish peroxidase and chymotrypsin. Only lactate dehydrogenase showed a dextran molecular weight-dependent decrease in V_{max} with the larger dextrans being the stronger uncompetitive inhibitor.

https://doi.org/10.1021/acsomega.1c03243
ACS Omega 2021, 6, 26239−26250

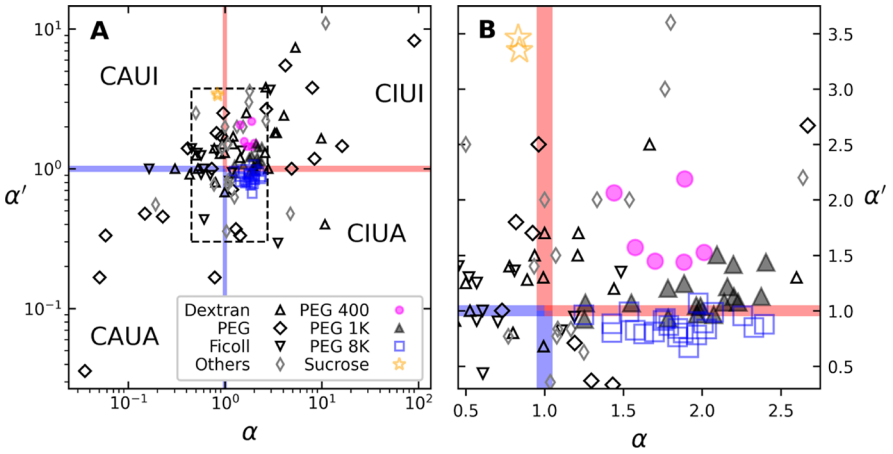

Figure 7. α and α' resulting from the presence of different cosolutes on different enzymes from Table S1 by Silverstein and Slade[5] (reproduced in Table S1 in Supporting Information) with selected results from this report. (A) α and α' plotted on a log scale. The cosolute concentration used by Silverstein and Slade[5] was between 300 and 400 g/L. The dextran, PEG, Ficoll, and other results were taken from Silverstein and Slade.[5] PEG 400, PEG 1 K, and PEG 8 K at concentrations 30−40 wt % and sucrose data at 24 wt % from this paper are also shown. The shaded blue and red cross mark α and α' between 0.95 and 1.05, which were taken to indicate no substantive change in α or α'. The red arms of the cross are for inhibition; α and $\alpha' > 1$ (horizontal and vertical, respectively). The blue components are for activation; α and $\alpha' < 1$ (horizontal and vertical, respectively). The labels CAUI, CIUI, CAUA, and CIUA mark the different mixed-behavior "quadrants" (Table 1). (B) Enlargement of the region marked by the dashed box in panel (A) using the same markers. Both α and α' were plotted on a linear scale.

Cosolutes' potential to stabilize or destabilize proteins provides another explanation for the changes in V_{max} and K_{asp}. While experimentally, the same volume of fresh enzyme was added to the solutions, cosolutes could stabilize or destabilize weakly folded CIAP present in the sample.[8,51] This would lead to an increase or decrease in E_t, causing V_{max} to rise or fall, respectively. Given the already mentioned extra interactions from PEG, this mode of operation could account for the mass dependence changes V_{max}. Many standard enzyme assay protocols often include albumin, typically at 0.1% concentration, as a stabilizing agent.[52] Also, in the case where there is little to no change in the underlying rate constants, k_1, k_{-1}, and k_{cat}, changes in E_t should also be directly reflected in K_{asp} (eqs 2 and 3). This could provide a simple explanation for CAUA and CIUI behavior where there are significant changes in both α and α'.

Recognizing that α and α' are kinetic parameters defined under initial rate and steady-state assumptions, it is not surprising that they exhibit nonlinearity as a function of wt % and log(Π). Data linearity is commonly seen in the crowding and the osmotic pressure literature, where experiments are largely conducted under equilibrium conditions. The outcomes of these types of experiments can be expressed as an equilibrium constant between two states, such as unfolded versus folded proteins and open versus closed channels. In these situations, linearity can be meaningfully interpreted through thermodynamics.[16]

Mechanistic Reason for the Prevalence of Cosolute-Induced Mixed-Behavior on Enzyme Kinetics. The observed cosolutes induced mixed behaviors on CIAP kinetics is consistent with other enzyme studies summarized by Silverstein and Slade.[5] Figure 7 shows α and α' calculated from 79 instances drawn from 30 studies on approximately 40 different enzymes using 12 different cosolutes where changes in K_M and V_{max} were reported in Table S1 from Silverstein and Slades.[5]

If α and α' between 0.95 and 1.05, indicated by the blue and red cross in Figure 7, respectively, are taken to represent "no changes" in step ① and ② kinetics, then, by far, the most common cosolute effect on enzyme kinetics was CIUI mixed behavior at 33% of the time (Figure S3 in Supporting Information). Overall, 77% of the time, the presence of cosolutes resulted in some sort of mixed behavior with pure competitive and uncompetitive behaviors accounting for the rest. The most "extreme" results reported by Silverstein and Slade[5] occurred from the presence of PEG, leading to CAUA and CIUI mixed behavior (Figure 7). As previously discussed, this could be simply attributed to large changes in E_t through stabilization or destabilization of weakly folded enzymes. Figure 7 also includes PEG 400, PEG 1 K, and PEG 8 K from this paper examined at similar concentrations, 30−40 wt %, to those compiled by Silverstein and Slade (300−400 g/L).[5] In this representation, the vertical stratification between the different PEGs examined emphasizes the various effects on step ② where PEG 400 acted as an inhibitor ($\alpha' > 1$) and PEG 8 K as an activator ($\alpha' < 1$).

The apparent common occurrence of cosolutes inducing mixed behavior across a wide variety of enzymes suggested a possible underlying general mechanism. To explain mixed inhibition, CIUI, of α-chymotrypsin caused by dextran, Pastor et al.[48] suggested product inhibition, where catalysis products exert an inhibitory effect through enzyme rebinding.[26] Although the initial-rate assumption used to derive the Michaelis−Menten equation removes the possibility of product rebinding, it is intuitive that product binding to the "original" free enzyme should result in competitive inhibition.[53] The greater challenge is understanding the mechanism of uncompetitive inhibition. Generally, small-molecule, uncompetitive inhibitors are less common compared to competitive inhibitors likely because they need to recognize and bind to a transient enzyme intermediate.[26,53] The hydrolysis of PNPP by CIAP occurs stepwise with the release of PNP and then followed by Pi.[54] In this double-displacement mechanism, further described below, PNP binding to the covalently modified CIAP would be the potential candidate for product-induced uncompetitive inhibition.

Although a distinguishing feature of mammalian AP, such as CIAP, is its uncompetitive inhibition by single amino acids

https://doi.org/10.1021/acsomega.1c03243
ACS Omega 2021, 6, 26239−26250

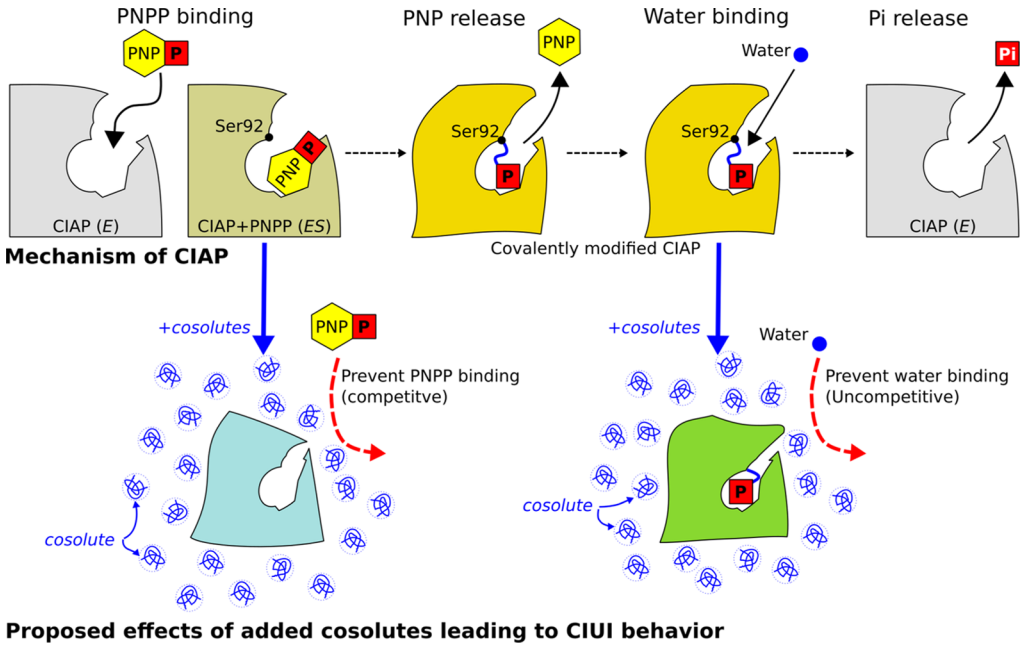

Figure 8. Mechanism of PNPP hydrolysis catalyzed by CIAP and how cosolutes could affect kinetics. Top row shows the double-displacement mechanism of hydrolysis of CIAP. PNPP binding to CIAP is followed by PNP release and covalent modification of Ser92 by phosphate. A water molecule then binds to the covalently modified CIAP, leading to Pi release and returning CIAP to its initial state. Bottom row shows one possible combination of cosolute effects on CIAP kinetics, leading into CIUI mixed behavior. The presence of cosolutes could prevent PNPP binding by collapsing the binding site. They could also induce additional conformational change preventing the water binding needed to release the covalently bound phosphate.

such as L-phe, PNP is unlikely an uncompetitive inhibitor in the presence of cosolutes. Both PNP and Pi are observed to be purely competitive inhibitors in traditional dilute solutions.[55] When cocrystallized with human placental AP, L-phe directly interacted with the negatively charged phosphorylated Ser92 through its positively charged amino terminus.[31,56] Binding of L-phe was further stabilized by interactions between its negatively charged carboxylic acid group and the surrounding basic amino acids such as Arg150 and Arg166. Bound this way, L-phe would block subsequent water-molecule binding, which provided a mechanistic explanation for its uncompetitive inhibition. Although further refinement of the original X-ray structure in the absence of L-phe[56] revealed a PNP bound near the catalytic site, its lack of charged groups similar to L-phe meant that it was located further away from the phosphorylated Ser92 and likely would not interfere with water binding.[31] A distal L-phe site, approximately 28 Å away from the catalytic site, was also observed.[31,56] Although PNP was observed to bind here, whether this site plays any role in inhibition is unclear. A further complication is that the effects of PNP product binding would need to be sensitive to cosolute identity and size. In the presence of PEG 8 K and 20 K, PNP acts as a competitive inhibitor and an uncompetitive activator, CIUA, while the other examined cosolutes generally behaved as CIUI inhibitors. In the presence of sucrose and dextran 6 K, its uncompetitive inhibition is even stronger. Assuming that cosolutes would neither alter the products of PNPP hydrolysis, PNP, and Pi, nor the double-displacement enzyme mechanism, a possible and challenging explanation would be to imagine the different cosolute inducing different CIAP conformations, enabling individual responses to PNP binding.

A proper explanation of the observed cosolute-induced mixed behavior on CIAP needs to take into account its specific double-displacement mechanism.[54] In double-displacement mechanisms,[26] substrates bind, PNPP and H_2O in the case of CIAP, sequentially and are interweaved between stepwise product release. At no point are all substrates bound to the enzyme, as implied in Figure 2.[54] For CIAP, this is diagrammed in the top row of Figure 8.

PNPP binding to CIAP results in cleavage of its ester bond, releasing the colored PNP into solution and leaving the phosphate covalently attached to Ser92, forming an intermediate enzyme state. In the next step, a water molecule binds to this covalently modified CIAP, which ultimately dephosphorylates Ser92, resetting CIAP to its original condition and ready to catalyze the hydrolysis of another PNPP molecule. Modifying PNPP or water molecule binding could lead to competitive or uncompetitive behaviors, ultimately resulting in mixed behaviors when both occur. The prevalence of the double-displacement mechanism in numerous other enzymes, such as trypsin, chymotrypsin, and lysozyme, provides an explanation for the widespread cosolute-induced mixed behavior.

Cosolute-induced changes in the vicinity of the enzyme active site, regardless of whether caused by crowding, confinement, or dehydration, would be an obvious means for altering substrate binding or product release in CIAP. Conformational changes resulting in steric obstruction of the catalytic site, from cleft closure, for example, would impede the enzyme−substrate complex and decrease k_1 (eq 2), leading to an increase in K_M, a decrease in K_{asp} (eq 3), competitive inhibition, all other rate constants, and E_t being the same.[20,21] Further cosolute-induced conformational changes to the covalently modified enzyme intermediate could slow entry of the mechanistically critical water molecule, lowering V_{max} by decreasing k_2 (eq 2) and leading to uncompetitive inhibition. Alternatively, observed uncompetitive inhibition could result from the steric hindrance of Pi release. A simultaneous

https://doi.org/10.1021/acsomega.1c03243
ACS Omega 2021, 6, 26239−26250

combination of these effects, one of which is diagrammed in the bottom row of Figure 8, provides a simple explanation for CIUI mixed inhibition in CIAP and suggests a framework for this most commonly observed mixed behavior. Pure competitive inhibition, on the other hand, could result from cosolutes only being able to induce sufficient conformational change to affect substrate binding but not enough to affect subsequent substrate binding such as H_2O in CIAP. Pure uncompetitive inhibition could be a result of a cosolute's ability to cause sufficient structural changes to block the second substrate binding step only after covalent modification. However, the same proposed conformational changes could also account for competitive and uncompetitive activation. Cleft closure around the active site could lower k_{-1} ES dissociation to a much greater extent than k_1, leading ultimately to an increase in K_{asp} and competitive activation through extra stabilization of the ES complex (eqs 2 and 3). Similarly, conformational modification of the covalently modified enzyme could increase the "residence" time when the water molecule stays "trapped" at the active site or enable quicker escape of Pi, leading to an increase in k_{cat} and uncompetitive activation. The additional steps involving water binding to the covalently modified state are not explicitly recognized in the simple Michaelis–Menten scheme (Figure 1). This suggests that a more comprehensive appreciation of how cosolutes influence enzyme kinetics needs to take into account their actual mechanistic steps.

CONCLUSIONS

1 Fitting initial velocity data to the K_{asp} and V_{max} form of the Michaelis–Menten equation (eq 4) offered numerous advantages compared to using the traditional K_M and V_{max} parameters (eq 1). Particularly, it led to insights into how cosolutes altered the individual steps of the classic Michaelis–Menten scheme (Figure 1) using ideas taken from small-molecule competitive and uncompetitive inhibition.

2 For PNPP hydrolysis catalyzed by CIAP, the carbohydrate cosolutes, dextran 6 K and sucrose, altered the kinetics of steps ① and ② (Figure 1) differently from the noncarbohydrate cosolutes, PEG's, TEG, and betaine. In step ①, all the noncarbohydrate cosolutes acted as competitive inhibitors. Comparatively, dextran 6 K and sucrose demonstrated little conclusive competitive inhibition and perhaps even slight activation. Cosolute effects on step ② displayed greater complexity. The observed uncompetitive behavior of the noncarbohydrates divided them into two groups. The large PEG's, PEG 20 K and PEG 8 K, acted as uncompetitive activators, increasing V_{max} of CIAP kinetics. The remaining smaller noncarbohydrate cosolutes behaved as uncompetitive inhibitors. Compared to these small noncarbohydrates, dextran 6 K and sucrose were much stronger uncompetitive inhibitors. Overall, PEG 20 K and PEG 8 K showed CIUA mixed behavior, while PEG 1 K, PEG 400, TEG, and betaine were CIUI mixed inhibitors. Dextran 6 K and sucrose demonstrated uncompetitive inhibition, but the significant decrease in V_{max} made it difficult to identify the form of competitive behavior, activating or inhibiting.

3 Using α and α' enabled quantifying cosolute effects on the two steps of the Michaelis–Menten scheme (Figure 1). In the case of CIAP, these two steps appeared to be influenced by different mechanisms.

(a). Step ①, enzyme–substrate complex formation, appeared to be more sensitive to osmotic stress than crowding. The noncarbohydrate cosolutes exhibited similar correlation in their α as a function of $\log(\Pi)$ with differences potentially resulting from size-dependent exclusion, a common observation in osmotic stress experiments. They also showed molecular weight independence in their concentration effects on α. Carbohydrates, considered to be more ideal crowders, showed weak competitive behavior consistent with the expected small volume change upon substrate binding.

(b). For step ②, product formation and release, the carbohydrate cosolutes exerted noticeably more potent uncompetitive inhibition versus noncarbohydrates. The latter showed distinct molecular weight-dependent behavior. PEG 20 K and PEG 8 K acted as uncompetitive activators. The smaller noncarbohydrates were uncompetitive inhibitors over the same osmotic pressure range. The great uncompetitive inhibition by dextran 6 K versus sucrose could be due to confinement. Although all this suggested that step ② in CIAP-catalyzed PNPP hydrolysis was sensitive to crowding, the question remains about the source of the volume change necessary for this mode of influence to be effective.

4 The generally observed mixed behavior induced by cosolutes on CIAP kinetics is consistent with the broader literature reviewed by Silverstein and Slade.[5] Cosolute-induced mixed behavior, CAUA, CAUI, CIUA, and CIUI, on enzyme kinetics was observed 77% of the time, with CIUI being the most common behavior at 33%. For CIAP, interference with or enhancement of water-binding after release of PNP could be a source of uncompetitive behavior. This double-displacement mechanism of CIAP is common in other enzymes. Alternatively, changes in E_t, through excluded volume, stabilizing or destabilizing weakly folded enzymes, would lead to parallel changes in V_{max} and K_{asp}, leading to CAUA or CIUI behavior. These possibilities could account for the widespread occurrence of cosolute-induced mixed behavior.

MATERIALS AND METHODS

CIAP Kinetic Assays. The hydrolysis of para-nitrophenyl phosphate (disodium salt from Sigma) by calf-IAP, CIAP (Worthington), was carried out in a reaction solution of 80 mM NaCl, 20 mM sodium borate buffer (pH 8.8), 2 mM $MgCl_2$, and 0.01 mM $ZnCl_2$. The cosolute solutions were made by weight percent, wt %, using the reaction solution as the solvent. The cosolutes, betaine, sucrose, dextran 6 K, TEG, and polyethylene glycol of molecular weight 400, 1, 8, and 20 K (PEG 400, PEG 1 K, PEG 8 K, and PEG 20 K) were all at least reagent grade. These cosolutes represent both carbohydrate and noncarbohydrate across a wide mass range. Sucrose was selected because it is a nonreducing sugar which removes the possibility of it covalently modifying CIAP. Betaine is a neutral zwitterionic osmolyte. Approximately 0.2 U of CIAP, prepared in a 50% glycerol/reaction solution (v/v), was added by a minimum volume (~1% of final volume) to both the uncrowded (i.e., dilute control) and crowded reaction solution.

https://doi.org/10.1021/acsomega.1c03243
ACS Omega 2021, 6, 26239–26250

The reaction was initiated by introducing a small volume (~1% of final volume) of freshly made PNPP dissolved in the reaction solutions to the reaction mixture to give a final substrate concentration. After quickly and gently mixing using a pipettor and/or a vortexer for more viscous solutions (i.e., PEG 8 K and PEG 20 K), the enzymatic formation of PNP was followed spectrophotometrically using a Cary 50 UV−vis set at λ = 400 nm. There was approximately a 30 s delay between initiating the reaction and the start of data collection. Data were typically collected in 1 s time-averaged intervals for 45 s and saved in a CSV-formatted file for analysis.

The normal daily experimental protocol consisted of preparing a fresh stock concentrated PNPP solution and CIAP. A "control" series (i.e., without cosolutes) was first done consisting of four PNPP substrate concentrations, between 0.1 and 1 mM, normally done in triplicate. This data was used to establish a control V_{max} and K_{asp} for that day. Using the same amount of enzyme and PNPP concentrations as in the control, kinetic experiments in the presence of cosolutes condition were conducted in the same manner to determine the apparent V_{max} and K_{asp} (V^*_{max} and K^*_{asp}). Calculating α and α' using measurements taken on the same day by the same investigator using the same solutions helped correct for changes in stock enzyme solutions and variabilities introduced by individual experimentalists. Experiments for each cosolute were conducted by at least two authors.

Data Analysis. CSV data from the Cary 50 was analyzed using Python within Jupyter Notebooks[57] online through Google Colaboratory[58] or locally installed. A linear fitting algorithm from the Python statsmodels module was used to determine the slope of the Abs_{400} versus time data (in seconds). These slopes were converted into initial velocities using our experimentally determined molar extinction coefficient of 1.79×10^5 M^{-1} cm^{-1}. The velocities versus initial PNPP concentrations were nonlinearly fitted to the Michaelis−Menten equation, eq 4 or 1, to determine V_{max} and K_{asp} or V_{max} and K_M, respectively, using the curve_fit routine from the scipy.optimize module. The curve_fit routine uses the Leveberg−Marquardt algorithm, which returns both the best-fit value and its standard deviation. Using control and apparent V_{max} and K_{asp}, the values of α and α' were determined for the crowded conditions (eq 5). The results of fitting data to both eqs 1 and 4 can be found in Supporting Information, AllData-KM-csv.txt and AllData-Kasp-csv.txt, respectively.

Osmotic Pressure Data. The osmotic pressure for all cosolutes except dextran 6 K was previously available at http://lpsb.nichd.nih.gov/osmotic_stress.htm, which is no longer accessible. A copy of that data and fits relevant for this paper can now be found at https://sites.google.com/mtroyal.ca/johnchik/osmotic-resource.

The logarithm of osmotic pressure data for each cosolute was fitted to the following function.

$$\log_{10}(\pi) = a + b \times (\text{wt \%})^c \quad (6)$$

where wt % is the weight % concentration of cosolute. The fitted a, b, and c results are shown in Table 3 below.

The dextran 6 K data was taken from dextran T10 fits published by Jonsson, as shown below.[35]

$$\pi(\text{in atm}) = 0.116 \times \text{wt \%} - 0.00491 \times (\text{wt \%})^2 + 0.000257 \times (\text{wt \%})^3 \quad (7)$$

Table 3. Resulting Fitted Parameters for Eq 6

cosolute	a	b	c	approximate Range of use (wt %)
betaine	3.90 ± 0.61	2.45 ± 0.59	0.16 ± 0.03	1−23
sucrose	4.29 ± 0.41	1.60 ± 0.37	0.21 ± 0.03	2−58
TEG	5.08 ± 0.16	1.26 ± 0.14	0.24 ± 0.02	2−50
PEG 400	5.25 ± 0.18	0.77 ± 0.15	0.33 ± 0.04	3−30
PEG 1 K	4.89 ± 0.39	0.79 ± 0.30	0.34 ± 0.07	3−60
PEG 8 K	3.90 ± 1.34	0.99 ± 0.96	0.36 ± 0.17	10−36
PEG 20 K	1.57 ± 0.44	2.75 ± 0.40	0.21 ± 0.02	2−48

Dextran T10 being larger in molecular weight than dextran 6 K (10 kDa vs 6 kDa) should yield an osmotic pressure smaller than actual. Figure S2 in Supporting Information shows the fit between the data and fit to eq 6 using the parameters Table 3 as well as eq 7.

■ ASSOCIATED CONTENT

Supporting Information

The Supporting Information is available free of charge at https://pubs.acs.org/doi/10.1021/acsomega.1c03243.

Histogram of the relative error in K_{asp}, K_M, and V_{max}, fit between log(Π) and wt % via eq 6 and the log(Π) of dextran T10 by Jonsson in eq 7,[35] the effects of the cosolute on enzyme kinetics measured by α and α' using data from Silverstein and Slade,[5] and a summary of their behaviors (PDF)

Determined V_{max} and K_{asp} values by fitting data to eq 4 (TXT)

Determined V_{max} and K_M values by fitting data to eq 1 (TXT)

■ AUTHOR INFORMATION

Corresponding Author

John K. Chik − *Department of Chemistry and Physics, Mount Royal University, Calgary, Alberta T2N4N1, Canada;* orcid.org/0000-0002-7314-3251; Email: jchik@mtroyal.ca

Authors

Oksana A. Yavorska − *Department of Chemistry and Physics, Mount Royal University, Calgary, Alberta T2N4N1, Canada*

Lukas Syriste − *Microbiology, Immunology & Infectious Diseases, Cumming School of Medicine, University of Calgary, Calgary, Alberta T3E 6K6, Canada*

Chantal M. du Plessis − *Department of Chemistry and Physics, Mount Royal University, Calgary, Alberta T2N4N1, Canada*

Maryam Yaqoob − *Department of Chemistry and Physics, Mount Royal University, Calgary, Alberta T2N4N1, Canada*

Kyle Loogman − *Department of Chemistry and Physics, Mount Royal University, Calgary, Alberta T2N4N1, Canada*

Michael Cordara − *Department of Chemistry and Physics, Mount Royal University, Calgary, Alberta T2N4N1, Canada*

Complete contact information is available at: https://pubs.acs.org/10.1021/acsomega.1c03243

Notes

The authors declare no competing financial interest.

All data, JupyterLab files, and Python scripts used in this report can be found at https://doi.org/10.5683/SP2/N7ZKXV (Mount Royal University Dataverse).

■ ACKNOWLEDGMENTS

The authors acknowledge the financial support from Mount Royal University's Internal Research Grant Fund and from the Faculty of Science and Technology's Innovation Grant, ESS Grant, Student Research Assistant Funding, and Petro-Canada Young Innovator Award. We also acknowlege Mount Royal University Library Open Access Fund for underwriting publication costs. Finally, we thank the faculty, staff, and students at Mount Royal University for their assistance and support.

■ REFERENCES

(1) Gierasch, L. M.; Gershenson, A. Post-Reductionist Protein Science, or Putting Humpty Dumpty Back Together Again. *Nat. Chem. Biol.* **2009**, *5*, 774−777.
(2) Ellis, R. J. Macromolecular Crowding: Obvious but Underappreciated. *Trends Biochem. Sci.* **2001**, *26*, 597−604.
(3) Zimmerman, S. B.; Trach, S. O. Estimation of Macromolecule Concentrations and Excluded Volume Effects for the Cytoplasm of Escherichia Coli. *J. Mol. Biol.* **1991**, *222*, 599−620.
(4) Bennett, B. D.; Kimball, E. H.; Gao, M.; Osterhout, R.; Van Dien, S. J.; Rabinowitz, J. D. Absolute Metabolite Concentrations and Implied Enzyme Active Site Occupancy in Escherichia Coli. *Nat. Chem. Biol.* **2009**, *5*, 593−599.
(5) Silverstein, T. P.; Slade, K. Effects of Macromolecular Crowding on Biochemical Systems. *J. Chem. Educ.* **2019**, *96*, 2476−2487.
(6) Balcells, C.; Pastor, I.; Pitulice, L.; Hernández, C.; Via, M.; Garcés, J. L.; Madurga, S.; Vilaseca, E.; Isvoran, A.; Cascante, M.; Mas, F. Macromolecular crowding upon in-vivo- like enzyme-kinetics: Effect of enzyme- obstacle size ratio http://newfrontchem.iqstorm.ro/upload/02-NFC-24-1_Balcells%20et%20al.pdf (accessed Aug 3, 2021).
(7) Vöpel, T.; Makhatadze, G. I. Enzyme Activity in the Crowded Milieu. *PLoS One* **2012**, *7*, No. e39418.
(8) Zhou, H.-X.; Rivas, G.; Minton, A. P. Macromolecular Crowding and Confinement: Biochemical, Biophysical, and Potential Physiological Consequences. *Annu. Rev. Biophys.* **2008**, *37*, 375−397.
(9) Minton, A. P. Excluded Volume as a Determinant of Macromolecular Structure and Reactivity. Biopolymers: Original Research on Biomolecules **1981**. *20*. 2093. DOI: 10.1002/bip.1981.360201006
(10) Minton, A. P.; Wilf, J. Effect of Macromolecular Crowding upon the Structure and Function of an Enzyme: Glyceraldehyde-3-Phosphate Dehydrogenase. *Biochemistry* **1981**, *20*, 4821−4826.
(11) Guin, D.; Gruebele, M. Weak Chemical Interactions That Drive Protein Evolution: Crowding, Sticking, and Quinary Structure in Folding and Function. *Chem. Rev.* **2019**, *119*, 10691−10717.
(12) Parsegian, V. A.; Rand, R. P.; Rau, D. C. [3] Macromolecules and water: Probing with osmotic stress. *Methods Enzymol.* **1995**, *259*, 43−94.
(13) Timasheff, S. N. The Control of Protein Stability and Association by Weak Interactions with Water: How Do Solvents Affect These Processes? *Annu. Rev. Biophys. Biomol. Struct.* **1993**, *22*, 67−97.
(14) Asakura, S.; Oosawa, F. On Interaction between Two Bodies Immersed in a Solution of Macromolecules. *J. Chem. Phys.* **1954**, *22*, 1255−1256.
(15) Sapir, L.; Harries, D. Is the Depletion Force Entropic? Molecular Crowding beyond Steric Interactions. *Curr. Opin. Colloid Interface Sci.* **2015**, *20*, 3−10.
(16) Parsegian, V. A.; Rand, R. P.; Rau, D. C. Osmotic Stress, Crowding, Preferential Hydration, and Binding: A Comparison of Perspectives. *Proc. Natl. Acad. Sci. U.S.A.* **2000**, *97*, 3987−3992.
(17) Parsegian, V. A.; Bezrukov, S. M.; Vodyanoy, I. Watching Small Molecules Move: Interrogating Ionic Channels Using Neutral Solutes. *Biosci. Rep.* **1995**, *15*, 503−514.
(18) Sidorova, N. Y.; Rau, D. C. Linkage of EcoRI Dissociation from Its Specific DNA Recognition Site to Water Activity, Salt Concentration, and pH: Separating Their Roles in Specific and Non-Specific Binding. *J. Mol. Biol.* **2001**, *310*, 801−816.
(19) Colombo, M.; Rau, D.; Parsegian, V. Protein Solvation in Allosteric Regulation: A Water Effect on Hemoglobin. *Science* **1992**, *256*, 655−659.
(20) Rand, R. P.; Fuller, N. L.; Butko, P.; Francis, G.; Nicholls, P. Measured Change in Protein Solvation with Substrate Binding and Turnover. *Biochemistry* **1993**, *32*, 5925−5929.
(21) Reid, C.; Rand, R. P. Probing Protein Hydration and Conformational States in Solution. *Biophys. J.* **1997**, *72*, 1022−1030.
(22) Dhar, A.; Samiotakis, A.; Ebbinghaus, S.; Nienhaus, L.; Homouz, D.; Gruebele, M.; Cheung, M. S. Structure, Function, and Folding of Phosphoglycerate Kinase Are Strongly Perturbed by Macromolecular Crowding. *Proc. Natl. Acad. Sci. U.S.A.* **2010**, *107*, 17586−17591.
(23) Currie, M.; Leopold, H.; Schwarz, J.; Boersma, A. J.; Sheets, E. D.; Heikal, A. A. Fluorescence Dynamics of a FRET Probe Designed for Crowding Studies. *J. Phys. Chem. B* **2017**, *121*, 5688−5698.
(24) Leopold, H. J.; Leighton, R.; Schwarz, J.; Boersma, A. J.; Sheets, E. D.; Heikal, A. A. Crowding Effects on Energy-Transfer Efficiencies of Hetero-FRET Probes As Measured Using Time-Resolved Fluorescence Anisotropy. *J. Phys. Chem. B* **2019**, *123*, 379−393.
(25) DeMoll, E.; Cox, D. J.; Daniel, E.; Riggs, A. F. Apparent Specific Volume of Human Hemoglobin: Effect of Ligand State and Contribution of Heme. *Anal. Biochem.* **2007**, *363*, 196−203.
(26) Cornish-Bowden, A. *Fundamentals of Enzyme Kinetics*; Wiley, 2013.
(27) Johnson, K. A. New Standards for Collecting and Fitting Steady State Kinetic Data. *Beilstein J. Org. Chem.* **2019**, *15*, 16−29.
(28) Manes, T.; Hoylaerts, M. F.; Müller, R.; Lottspeich, F.; Hölke, W.; Millán, J. L. Genetic Complexity, Structure, and Characterization of Highly Active Bovine Intestinal Alkaline Phosphatases. *J. Biol. Chem.* **1998**, *273*, 23353−23360.
(29) Hoylaerts, M. F.; Manes, T.; Millán, J. L. Molecular Mechanism of Uncompetitive Inhibition of Human Placental and Germ-Cell Alkaline Phosphatase. *Biochem. J.* **1992**, *286*, 23−30.
(30) Hoylaerts, M. F.; Manes, T.; Millán, J. L. Mammalian Alkaline Phosphatases Are Allosteric Enzymes. *J. Biol. Chem.* **1997**, *272*, 22781−22787.
(31) Stec, B.; Cheltsov, A.; Millán, J. L. Refined Structures of Placental Alkaline Phosphatase Show a Consistent Pattern of Interactions at the Peripheral Site. *Acta Crystallogr., Sect. F: Struct. Biol. Cryst. Commun.* **2010**, *66*, 866−70.
(32) Millán, J. L. Alkaline Phosphatases. *Purinergic Signal.* **2006**, *2*, 335.
(33) Besman, M.; Coleman, J. E. Isozymes of Bovine Intestinal Alkaline Phosphatase. *J. Biol. Chem.* **1985**, *260*, 11190−11193.
(34) Sekiguchi, S.; Hashida, Y.; Yasukawa, K.; Inouye, K. Effects of Amines and Aminoalcohols on Bovine Intestine Alkaline Phosphatase Activity. *Enzyme Microb. Technol.* **2011**, *49*, 171−176.
(35) Jonsson, G. Boundary Layer Phenomena during Ultrafiltration of Dextran and Whey Protein Solutions. *Desalination* **1984**, *51*, 61−77.
(36) Homchaudhuri, L.; Sarma, N.; Swaminathan, R. Effect of Crowding by Dextrans and Ficolls on the Rate of Alkaline Phosphatase-Catalyzed Hydrolysis: A Size-Dependent Investigation. *Biopolymers* **2006**, *83*, 477−486.
(37) Iino, S.; Fishman, L. The Effect of Sucrose and Other Carbohydrates on Human Alkaline Phosphatase Isoenzyme Activity. *Clin. Chim. Acta* **1979**, *92*, 197−207.
(38) Boulanger, R. R., Jr; Kantrowitz, E. R. Characterization of a Monomeric Escherichia Coli Alkaline Phosphatase Formed upon a Single Amino Acid Substitution. *J. Biol. Chem.* **2003**, *278*, 23497−23501.

(39) Vodyanoy, I.; Bezrukov, S. M.; Parsegian, V. A. Probing Alamethicin Channels with Water-Soluble Polymers. Size-Modulated Osmotic Action. *Biophys. J.* **1993**, *65*, 2097−2105.
(40) Stanley, C.; Krueger, S.; Parsegian, V. A.; Rau, D. C. Protein Structure and Hydration Probed by SANS and Osmotic Stress. *Biophys. J.* **2008**, *94*, 2777−2789.
(41) Parsegian, V. A.; Rand, R. P.; Rau, D. C. Macromolecules and Water: Probing with Osmotic Stress. *Methods in Enzymology*; Academic Press, 1995; Vol. *259*, pp 43−94.
(42) Winzor, D. J.; Wills, P. R. Molecular Crowding Effects of Linear Polymers in Protein Solutions. *Biophys. Chem.* **2006**, *119*, 186−195.
(43) Tubio, G.; Nerli, B.; Picó, G. Relationship between the Protein Surface Hydrophobicity and Its Partitioning Behaviour in Aqueous Two-Phase Systems of Polyethyleneglycol−dextran. *J. Chromatogr. B* **2004**, *799*, 293−301.
(44) Bekale, L.; Agudelo, D.; Tajmir-Riahi, H. A. The Role of Polymer Size and Hydrophobic End-Group in PEG−protein Interaction. *Colloids Surf. B Biointerfaces* **2015**, *130*, 141−148.
(45) Wu, J.; Zhao, C.; Lin, W.; Hu, R.; Wang, Q.; Chen, H.; Li, L.; Chen, S.; Zheng, J. Binding Characteristics between Polyethylene Glycol (PEG) and Proteins in Aqueous Solution. *J. Mater. Chem. B* **2014**, *2*, 2983−2992.
(46) Rong, Y. Probing the Structure of Dextran Systems and Their Organization; Rutgers University-Graduate School-New Brunswick, 2008.
(47) Squire, P. G. Calculation of Hydrodynamic Parameters of Random Coil Polymers from Size Exclusion Chromatography and Comparison with Parameters by Conventional Methods. *J. Chromatogr. A* **1981**, *210*, 433−442.
(48) Pastor, I.; Vilaseca, E.; Madurga, S.; Garcés, J. L.; Cascante, M.; Mas, F. Effect of Crowding by Dextrans on the Hydrolysis of N-Succinyl-L-Phenyl-Ala-P-Nitroanilide Catalyzed by Alpha-Chymotrypsin. *J. Phys. Chem. B* **2011**, *115*, 1115−1121.
(49) Wenner, J. R.; Bloomfield, V. A. Crowding Effects on Eco RV Kinetics and Binding. *Biophys. J.* **1999**, *77*, 3234−3241.
(50) Pastor, I.; Pitulice, L.; Balcells, C.; Vilaseca, E.; Madurga, S.; Isvoran, A.; Cascante, M.; Mas, F. Effect of Crowding by Dextrans in Enzymatic Reactions. *Biophys. Chem.* **2014**, *185*, 8−13.
(51) Timasheff, S. N. Control of Protein Stability and Reactions by Weakly Interacting Cosolvents: The Simplicity of the Complicated. *Adv. Protein Chem.* **1998**, *51*, 355−432.
(52) *Albumin, in Worthington Enzyme Manual 280*; Worthington, K.; Worthington, V., Eds., 1993; p 13.
(53) Purich, D. L. *Enzyme Kinetics : Catalysis & Control : A Reference of Theory and Best-Practice Methods*; Elsevier Academic ; Elsevier Science [distributor]: San Diego, Calif.; Oxford, 2010.
(54) Stec, B.; Holtz, K. M.; Kantrowitz, E. R. A Revised Mechanism for the Alkaline Phosphatase Reaction Involving Three Metal Ions. *J. Mol. Biol.* **2000**, *299*, 1303−1311.
(55) Dean, R. L. Kinetic Studies with Alkaline Phosphatase in the Presence and Absence of Inhibitors and Divalent Cations. *Biochem. Mol. Biol. Educ.* **2002**, *30*, 401−407.
(56) Llinas, P.; Stura, E. A.; Ménez, A.; Kiss, Z.; Stigbrand, T.; Millán, J. L.; Le Du, M. H. Structural Studies of Human Placental Alkaline Phosphatase in Complex with Functional Ligands. *J. Mol. Biol.* **2005**, *350*, 441−451.
(57) Kluyver, T.; Ragan-Kelley, B.; Pérez, F.; Granger, B.; Bussonnier, M.; Frederic, J.; Kelley, K.; Hamrick, J.; Grout, J.; Corlay, S.; Ivanov, P.; Avila, D.; Abdalla, S.; Willing, C. Jupyter development team. Jupyter Notebooks − a Publishing Format for Reproducible Computational Workflows. In *Positioning and Power in Academic Publishing: Players, Agents and Agendas*; Loizides, F., Scmidt, B., Eds.; IOS Press, 2016; pp 87−90.
(58) Google Colaboratory https://colab.research.google.com/notebooks/intro.ipynb?utm_source=scs-index (accessed Sept 26, 2021).

https://doi.org/10.1021/acsomega.1c03243
ACS Omega 2021, 6, 26239−26250